IEEE Access
Multidisciplinary | Rapid Review | Open Access Journal

Received June 6, 2018, accepted July 20, 2018, date of publication July 31, 2018, date of current version August 20, 2018.

Digital Object Identifier 10.1109/ACCESS.2018.2861468

Three-Dimensional Path Planning for AUV Based on Interfered Fluid Dynamical System Under Ocean Current (June 2018)

PENG YAO AND SHIQIANG ZHAO
College of Engineering, Ocean University of China, Qingdao 266100, China
Corresponding author: Shiqiang Zhao (zsqouc@163.com)

This work was supported in part by the China Postdoctoral Science Foundation under Grant 2017M622278, in part by the Natural Science Foundation of Shandong Province, China, under Grant ZR2018BF016, and in part by the Fundamental Research Funds for the Central Universities under Grant 201713046.

ABSTRACT This paper focuses on planning a three-dimensional (3-D) path for the autonomous underwater vehicle in ocean environment with complicated static and dynamic obstacles as well as the ocean current. Imitating the principle of natural flow avoiding rocks, we develop a submerged path planning method based on improved interfered fluid dynamical system (IIFDS). In view of the particular feature of ocean environment, the obstacles and ocean current are modeled first. The flow field weight coefficient is then proposed to add the current into the confluence of IIFDS, so that the planned path could make use of the current. In order to obtain the energy-optimal path, the improved genetic algorithm whose mutation operator is modified by grey wolf optimizer is proposed to optimize the repulsive and tangential reaction coefficient, tangential direction coefficient, and flow field weight coefficient. Furthermore, a reverse-avoidance strategy is applied to real-time path planning to avoid dynamic obstacles, combined with IIFDS. Finally, the good performance of our proposed method is verified by simulations in various scenarios.

INDEX TERMS Three-dimensional path planning, interfered fluid dynamical system (IFDS), ocean current, improved genetic algorithm (IGA), dynamic obstacles.

I. INTRODUCTION

The geographical and hydrological environment in the ocean is complex and uncertain, including undulating terrain, current and enemy torpedoes, etc. Path planning plays a vital role in the intelligence of autonomous underwater vehicle (AUV) and is the key to successful, efficient and safe completion of missions. It should plan an optimal path from the starting point to the destination while avoiding kinds of obstacles. Compared with 2-D path planning methods, 3-D path planning methods are more complicated but more flexible and feasible. The main difference between underwater robots and other robots' path planning is that the submerged planning needs to take the complexity of ocean into account. In addition to the obstacles, ocean current could easily have an influence on underwater vehicles[1].

A large number of experts in this field have already conducted a variety of researches. Rapidly exploring random tree (RRT) was used to plan paths and could obtain collision-free paths in a short time [2]. Reference [3] combined the genetic algorithm (GA) with particle swarm optimization (PSO) to obtain the quasi-optimal 3-D paths in complex situations. With the help of ''single-program, multiple-data'' parallel programming paradigm, it improved the calculating speed on multicore CPUs. A potential field obstacle avoidance algorithm based on the fluid mechanics panel methods was introduced in [4] to avoid obstacles in 3-D space. Reference [5] developed a method for constructing risk-maps using automatic information systems, based on the A* algorithm, in order to find the minimum risk path between the specified start and target position. It reduces the risk of collision at the expense of efficiency. A novel fast marching (FM) algorithm which absorbs the high efficiency of A* and the accuracy of the FM algorithm was applied to extracting the continuous path in a 2-D discrete environment. And multi-resolution method was introduced to improve the planning efficiency [6]. Even though these methods have laid out feasible paths, they have not been applied to the

marine environment. The ocean current has not been considered or only the uncertainty caused by ocean current has been taken into consideration. However, the AUV path planning usually takes the ocean current into account.

Reference [7] introduced two stochastic planners, *a Minimum Expected Risk planner* and *a risk-aware Markov Decision Process,* to utilize the forecasting of current probabilistically. It helps to improve the safety and reliability of AUV navigation in coastal regions. Reference [8] developed a new modified level set equation to plan a 2-D path. The horizontal flow is combined with the standard vehicle motion, and the time-optimal paths in continuous dynamic flows are obtained by solving the particle tracking equation backwards. Reference [9] adopted a method based on partial differential equations to obtain a 2-D time-optimal path and it requires to make full use of ocean current. Reference [10] proposed an approach based on annular space decomposition (ASD) for AUV, which can be applied in turbulent, cluttered and uncertain environments. This method decomposes the space into annular areas and generates trajectories in each annular area. On the basis of ASD, [11] presented an optimal and efficient path planner based on a shell space decomposition (SSD) scheme. Instead of the annuli in a 2-D plane, the shells were used to define the volumes and obtain paths in a 3-D space. With the help of quantum-behaved particle swarm optimization (QPSO) planner, it figured out the optimal path that could bypass the upstream flow and exploit the downstream flow. This type of literature considers the utilization of ocean current and the uncertainty of the marine environment while planning underwater paths. It is no denying that they have higher practicality. Nevertheless, there are also some problems. For example, it is difficult to fully consider the requirements of path feasibility, optimality and complex environmental constraints. They have problems such as local extreme points, excessive calculations and 2-D limitation.

In addition to static obstacles, there are many unknown dynamic threats in the actual marine environment, such as large-scale oceanic lives, enemy torpedoes, submarines, etc. Reference [12], [13] realized real-time avoidance of single or multiple obstacles of the manipulator by using a dynamic system (DS) method. Velocity Change Space (VCS) was established in [14] by using the velocity and direction change of the robot as axes, and the motion planning problem of mobile robots avoiding dynamic threats was discussed in this space. Reference [15] described a fast path planning method suitable for avoiding moving obstacles by using Laplace potential. However, most of these literatures are used for mobile robots or robotic arms to avoid small obstacles. Few studies are applied to avoiding dynamic threats in underwater space. Reference [16] considered the static and dynamic threats in the spatiotemporal current vectors, using the evolutionary algorithm (EA) to plan the 3-D rendezvous path. Reference [17] proposed a 2-D path re-planning algorithm combined with EA and was applied to a cluttered environment with moving obstacles.

Inspired by the natural phenomena that flowing water could avoid obstacles, Wang *et al.* [18] proposed a path planning algorithm based on interfered fluid dynamical system (IFDS) which was applied to the unmanned aerial vehicle (UAV) path planning. In response to the existence of stagnation points and trap areas, the improved IFDS (IIFDS) was hence employed [19]. It has the advantages of low computational complexity, suitability for 3-D space and good path quality. Based on this method, we plan the path for AUV in 3-D marine environment in this paper. We not only consider the complex static obstacles of the seabed, but also introduce ocean current into the initial convergence of the IIFDS algorithm in a certain proportion so that the algorithm could utilize the current simultaneously. Improved GA (IGA) incorporating grey wolf optimization (GWO) is used to optimize the feasible path. The length of path and the angle between AUV and current are included in the fitness function, in order to get the energy-optimal, feasible and efficient path. In the end, the IIFDS combined with the reverse-avoidance strategy is used for real-time path planning to avoid possible dynamic threats.

The remaining paper is organized as follows. Section 2 describes the IIFDS method. In Section 3, ocean current is added to the IIFDS. IGA for path optimization is presented in Section 4. Dynamic threats are considered in Section 5. Section 6 describes the simulation results. Finally, the conclusion is drawn in Section 7.

II. DESCRIPTION OF STANDARD IIFDS METHOD

A. OBSTACLE MODEL

The high-quality environment model is the precondition and the basis of path planning work. In order to balance the accuracy with the efficiency, this paper adopts a unified standard model to represent various irregular obstacles [19]. Obstacles are extracted from the typical feature points for envelope processing. The equivalent are standard convex polyhedrons and the obstacles can be expressed as (1).

$$\Gamma(x, y, z) = \left(\frac{x - x_0}{\tau a}\right)^{2p} + \left(\frac{y - y_0}{\tau b}\right)^{2q} + \left(\frac{z - z_0}{\tau c}\right)^{2r} \tag{1}$$

where $P = (x, y, z)$ is the position. The complex terrain generated by simulation in MATLAB is shown in Fig.1. Then the description of any obstacle in the actual environment can be simplified to select a suitable envelope by adjusting the coefficients.

B. IIFDS FORMULATION

The IFDS algorithm imitates the property of flowing water and establishes the basic model of path planning: the undisturbed flowing water is regarded as the initial flow field; the stones are regarded as obstacles; the flowing water that bypasses the stone is regarded as the disturbed flow field; the disturbed flow field line is regarded as the planning path. When there is no obstruction in the planning area, the AUV

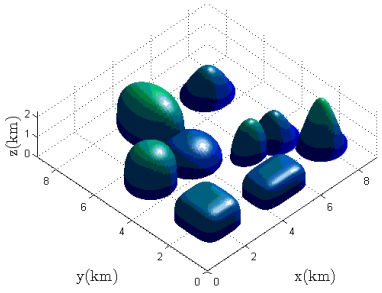

FIGURE 1. Simulated 3-D topographic map.

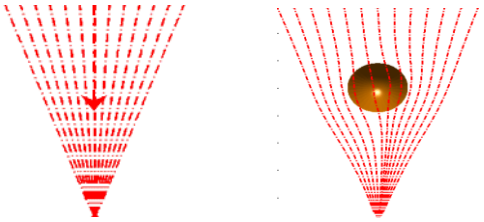

FIGURE 2. Illustration of convergence. (a) Undisturbed convergence. (b) Disturbed convergence.

can reach the target point along the straight line of the confluence (Fig.2 (a)). In contrast, when there are obstacles in the area, the flow field of the confluence will change its original straight state due to obstacles, but it can still smoothly bypass the obstacles and eventually converge to the target point (Fig.2 (b)).

By using the matrix to represent the disturbed effect of obstacles on the flow field, the disturbed flow field which helps to get the planning path can be obtained. First, we establish the initial flow field model without obstacle, i.e., the convergence:

$$\mathbf{U}(P) = -\left(\frac{V_0 \cdot (x - x_d)}{d(P, P_d)} \quad \frac{V_0 \cdot (y - y_d)}{d(P, P_d)} \quad \frac{V_0 \cdot (z - z_d)}{d(P, P_d)}\right)^T \tag{2}$$

where V_0 is a virtual interval with no practical significance, $f(P, P_d)$ is the Euclidean distance between the current AUV position P and the target position P_d:

$$d(P, P_d) = \sqrt{(x - x_d)^2 + (y - y_d)^2 + (z - z_d)^2} \tag{3}$$

Assuming that the number of known obstacles is K, the disturbance influence of obstacles on the confluence can be expressed as a matrix:

$$\overline{\mathbf{M}}(P) = \sum_{k=1}^{K} \omega_k(P)\mathbf{M}_k(P) \tag{4}$$

where $\omega_k(P)$ is the disturbance coefficient, $\overline{\mathbf{M}}(P)$ is the disturbance matrix:

$$\omega_k(P) = \begin{cases} 1 & K = 1 \\ \prod\limits_{i=1, i\neq k}^{K} \dfrac{\Gamma_i(P) - 1}{(\Gamma_i(P) - 1) + (\Gamma_k(P) - 1)} & K \neq 1 \end{cases} \tag{5}$$

$$\omega_k(P) = \frac{\omega_k(P)}{\sum\limits_{k=1}^{K} \omega_k(P)} \tag{6}$$

$$\mathbf{M}_k(P) = \mathbf{I} - \frac{\mathbf{n}_k(P) \cdot \mathbf{n}_k(P)^T}{|\Gamma_k(P)|^{\frac{1}{\rho_k}}\, \mathbf{n}_k(P)^T \mathbf{n}_k(P)} + \frac{\mathbf{t}_k(P) \cdot \mathbf{n}_k(P)^T}{|\Gamma_k(P)|^{\frac{1}{\sigma_k}}\, |\mathbf{t}_k(P)|\, |\mathbf{n}_k(P)|} \tag{7}$$

$$\rho_{\mathrm{k}} = \rho_k^0 \cdot e^{\left(1 - \frac{1}{d(\mathrm{P},\mathrm{P_d}) d(\mathrm{P},\mathrm{O_k})}\right)} \tag{8}$$

$$\sigma_k = \sigma_k^0 \cdot e^{\left(1 - \frac{1}{d(P,P_d) d(P,O_k)}\right)} \tag{9}$$

$$t_k(P) = R_k t_k'(P) \tag{10}$$

where $\Gamma(P)$ is the obstacle function, $\mathbf{I}$ is a third-order identity matrix, $\rho_k^0 > 0$ is repulsive reaction coefficient of obstacle k, $\sigma_k^0 > 0$ is tangential reaction coefficient, R_k represents the coordinate rotation matrix of the coordinate system $O'\_x'y'z'$ to O_xyz, $d(P, P_d)$ is the distance between the AUV and the destination, $d(P, O_{\mathrm{k}})$ is the distance between the AUV and the surface of the kth obstacle, $\mathbf{n}_k(P)$ which is perpendicular to the obstacle surface outward is the radial normal vector of the kth obstacle:

$$\mathbf{n}_k(P) = \begin{bmatrix} \frac{\partial \Gamma_k(P)}{\partial x} & \frac{\partial \Gamma_k(P)}{\partial y} & \frac{\partial \Gamma_k(P)}{\partial z} \end{bmatrix}^T \tag{11}$$

Construct a coordinate system $O'\_x'y'z'$ on a tangential plane S which is perpendicular to $\mathbf{n}_k(P)$ with $\mathbf{n}_k(P)$ as the z'-axis. The x'-axis and the y'-axis are:

$$\begin{cases} x' = \begin{bmatrix} \frac{\partial \Gamma_k(P)}{\partial y} & -\frac{\partial \Gamma_k(P)}{\partial x} & 0 \end{bmatrix}^T \\ y' = \begin{bmatrix} \frac{\partial \Gamma_k(P)}{\partial x} \cdot \frac{\partial \Gamma_k(P)}{\partial z} & \frac{\partial \Gamma_k(P)}{\partial y} \cdot \frac{\partial \Gamma_k(P)}{\partial z} \\ -\left(\frac{\partial \Gamma_k(P)}{\partial x}\right)^2 & -\left(\frac{\partial \Gamma_k(P)}{\partial y}\right)^2 \end{bmatrix}^T \end{cases} \tag{12}$$

$\mathbf{t}_{\mathrm{k}}'(P) = \begin{bmatrix} \cos\theta_k & \sin\theta_k & 0 \end{bmatrix}^T$ is any tangent vector on the S plane, $\theta_k \in [-\pi, \pi]$ is the tangential direction coefficient which represents the angle between $\mathbf{t}_{\mathrm{k}}'$ and the x'-axis.

The final disturbance flow velocity is:

$$\begin{aligned} \overline{\mathbf{U}}(P) = \overline{\mathbf{M}}(P)\mathbf{U}(P) &= \sum_{k=1}^{K} \omega_k(P)\mathbf{M}_k(P)\overline{\mathbf{U}}(P) \\ &= \sum_{k=1}^{K} \omega_k(P)\overline{\mathbf{U}}_k(P) \end{aligned} \tag{13}$$

The path can be obtained through integrating the velocity:

$$P_{i+1} = P_i + \overline{\mathbf{U}}(P)\Delta t \tag{14}$$

and $\overline{\mathbf{U}}_k(P)$ is the disturbed flow velocity of the kth obstacle at the point P, Δt is the step length and the smaller the value is, the more accurate the path is but the greater the amount of calculation is. This method accords with the general characteristics of flowing water:

a) The path satisfies the terrain boundary constraints, and the disturbance flow velocity does not point to the obstacle's radial normal vector, i.e., the path has the characteristics of following obstacles, but will never pass through the interior of the obstacles;
b) The path finally converges to the destination, i.e., the underwater robot can reach the destination;
c) There is no local extreme point outside of the obstacles which will prevent the AUV from moving;

These characteristics have been demonstrated in [19].

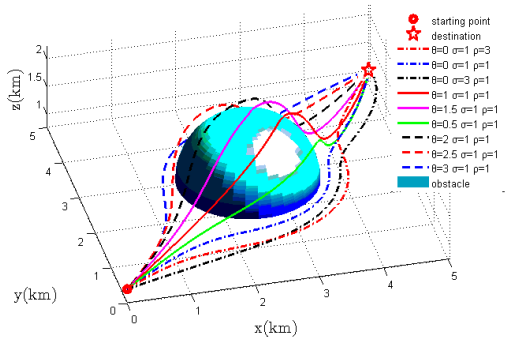

FIGURE 3. Paths distribution with different coefficients.

Fig.3 shows a variety of feasible paths planned by the IIFDS to avoid a single obstacle. The effect of each coefficient on the path can be roughly summarized as follows: The tangential direction coefficient θ_k determines the plane where the path lies. The closer the θ_k approaches $0, \pi, -\pi$, the closer the streamlines are to the horizontal plane, i.e., the AUV tends to avoid obstacles from the side. As θ_k approaches $\pi/2$, the streamlines become closer to the vertical plane, i.e., AUV tends to bypass obstacles from above. The larger ρ and σ is, the earlier the path avoids obstacles, the farther away from the obstacles is and the safer the path is. But the length of path may increase, which is not conducive to saving energy. In general, the IIFDS can safely and smoothly avoid all obstacles by selecting appropriate combination of coefficients.

III. IIFDS METHOD UNDER OCEAN CURRENT

The rational use of ocean current can not only increase the navigational power of AUV and save the energy consumption, but also ensure the safety of vehicles and contribute to improving the concealment. One of the advantages of IIFDS is that it can be modeled for specific situations. With respect to the impact of current, we consider adding a proportion of its velocity $\mathbf{V}$ to the initial flow field $\mathbf{U}$ to construct a new convergence $\mathbf{W}$:

$$\mathbf{W} = \lambda\mathbf{U} + (1-\lambda)\mathbf{V} \tag{15}$$

where $\lambda \in [0, 1]$ is called the flow field weight coefficient, which determines the proportion of the current and the initial flow in the new convergence. Convergence determines the basic direction of the path. Through the introduction of the λ, on one hand the AUV moves toward the target point, on the other hand it is affected by the current. As a result, when the current is helpful, λ can take a smaller value so that AUV can save energy by drifting along the current as much as possible. On the contrary, when the current is unusable and even affects the navigation and safety of AUV, λ can take a higher value.

This paper assumes the current during the course is time-stable, i.e., the magnitude and direction of the current velocity at each point at different instants of time are constant. And relative to the horizontal movement, the current in the vertical direction can be neglected. The current in the horizontal plane can be expressed by the stream function [20] shown in (16).

$$F(x, y, t) = 1 - \tanh\left(\frac{y - b(t)\cos[k(x - ct)]}{\sqrt{1 + k^2 b^2(t)\sin^2[k(x - ct)]}}\right) \tag{16}$$

$$b(t) = b_0 + e\cos(\varpi t + \chi) \tag{17}$$

Different meandering current can be obtained by adjusting the parameters. The current described by this function is also related to time and will change as the time changes. Since we suppose the current is constant, t takes a fixed value. When $t = 3$, $c = 1.2$, $k = 0.8$, $e = 0.1$, $b_0 = 2.2$, $\varpi = 0.4$, $\chi = \pi/2$, the flow field is shown in Fig.5. According to this stream function, the velocity in the x and y directions at the point (x, y) can be obtained. The velocity in each direction is still a function of x, y, and t:

$$\begin{cases} V_x(x, y, t) = -\dfrac{\partial F}{\partial y} \\ V_y(x, y, t) = \dfrac{\partial F}{\partial x} \end{cases} \tag{18}$$

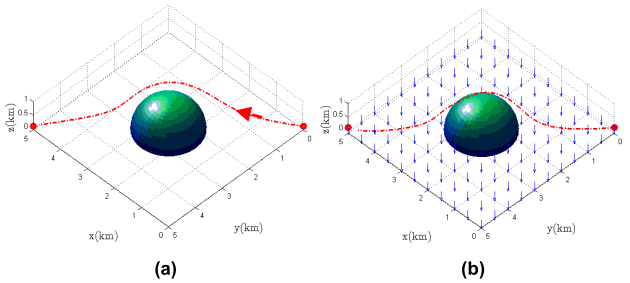

FIGURE 4. The influence of current on the safety of AUV navigation. (a) No current. (b) Affected by current.

where V_x, V_y are x, y velocities respectively. The velocity obtained here is the relative speed whose maximum value is 1, so it should be multiplied by the maximum value of the actual current speed during application. Fig.4 (a) illustrates the planned path when there is no current, whereas (b) illustrates the planned path when the current velocity is $(-0.25, 0.25, -0.5)$ m/s, the initial flow field velocity is 1.5 m/s, $\lambda = 0.5$. It is obvious that the path under the influence of ocean current is too close to the obstacle. Therefore, if we

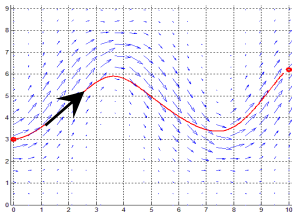

FIGURE 5. Meandering current and the path that utilizes the current.

do not make appropriate adjustments or optimization to the path when there is current, it may not only result in excessive energy consumption, but also make the path infeasible. On the contrary, if we select the flow field weight coefficient λ reasonably in some cases to make the AUV sail along the current, it can save energy or increase the speed of navigation (Fig.5).

IV. PATH OPTIMIZATION

The coefficients of IIFDS are selected randomly in the above section, so some paths may be too long or too close to obstacles or influenced by current which could make the path infeasible. Therefore, the optimization of coefficients is also discussed. GA are widely used because of its implicit parallelism and strong global optimization ability.

A. GA

1) ENCODING

The different paths generated by the IIFDS algorithm are determined by the three coefficients in the original algorithm and the flow field weight coefficient that is added after consideration of the ocean current, so the four coefficients are selected as GA chromosomes, and floating-point numbers are used for encoding. The chromosome of an individual is $C = \{\rho, \theta, \sigma, \lambda\}$ denoting repulsive reaction coefficient, tangential direction coefficient, tangential reaction coefficient, flow field weight coefficient respectively.

2) INITIALIZATION

Initialize a population that contains multiple individuals $G(g) = \{C_1, C_2, \ldots C_n\}$, $g = 1$, where g is the number of iterations, n is the number of individuals in the population (20-200) to ensure the diversity of chromosome. The randomly generated coefficients are constrained according to (19).

$$\begin{cases} 1 \le \rho \le \rho_{\max} \\ 0 \le \theta \le \pi \\ 1 \le \sigma \le \sigma_{\max} \\ 0 \le \lambda \le 1 \end{cases} \tag{19}$$

where $\rho_{\max}$ and $\rho_{\max}$ are maximum values of repulsive reaction coefficient and tangential reaction coefficient respectively.

3) FITNESS FUNCTION

While AUV is free from cable constraints, limited energy has become the primary factor limiting its path planning. How to save energy should be the primary considered question especially under the influence of ocean current, so we choose energy consumption as the fitness value. Assuming that the speed of AUV's external performance is constant, the energy consumption is mainly related to the length of the path, the angle between the AUV velocity and the current velocity. The fitness function A is defined as:

$$A = \eta_1 A_1 + \eta_2 A_2 \tag{20}$$

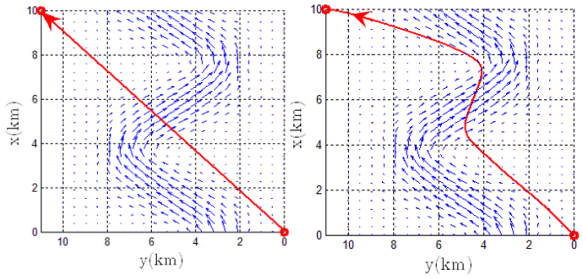

FIGURE 6. Paths focusing on different costs. (a) Emphasis on short paths. (b) Emphasis on downstream paths.

where A_1 is the cost of path length, A_2 is the cost of angle between the AUV velocity and the current velocity, η_1, η_2 are the corresponding weight coefficients. By choosing different weight coefficients, the importance of the path length and ocean current can be changed. The higher the value of η_1/η_2 is, the more emphasis is placed on the path length. In this situation, the planned path is biased towards Fig.6 (a). Otherwise, the emphasis is placed on saving energy with the help of current and the path is more biased towards Fig.6 (b). Section 6 will specifically analyze the relationship between η_1, η_2 and the path through simulation.

Set the AUV starting point as $P_s = (x_s, y_s, z_s)$, the target point as $P_d = (x_d, y_d, z_d)$, the waypoint as $P_w = (x_w, y_w, z_w)$, then the collection of all points on the path can be expressed as $\{P_1, P_2 \ldots P_w \ldots P_W\}$, where W is the number of points and $P_1 = P_s$, $P_W = P_d$. Define A_1 as the sum of Euclidean distances between waypoints:

$$A_1 = \sum_{w=2}^{W} |P_w - P_{w-1}| \tag{21}$$

According to the principle of dynamics, a downstream path is more conducive to saving energy or saving time for AUV [20], [21]. We use the angle between AUV and current's velocity to determine the degree of downstream, with the following definition of A_2:

$$A_2 = \frac{\sum_{w=1}^{W} \left[\arccos\left(\frac{U_w^T \cdot V}{|U_w||V|}\right)\right]}{W} \tag{22}$$

where U_w is the velocity along the wth path segment, V is the constant current velocity. When U_w and V are in the same direction, i.e., the included angle is 0°, $A_2 = 0$. As the angle

increases, the AUV gradually reverses the flow. When U_w and V are completely reversed, $A_2 = \pi$. And the lower the value of A_2 is, the more the AUV tends to sail downstream and the higher the fitness is.

In some cases, if only energy consumption is used as the fitness, the planned path may be too close to the obstacles in order to save energy. We hence introduce the safety cost:

$$A_3 = \sum_{k=1}^{K} A_3^k \tag{23}$$

$$A_3^k = \begin{cases} \infty & \Gamma_k(P) \le 1 \\ 0 & \Gamma_k(P) > 1 \end{cases} \tag{24}$$

$\Gamma_k(P) \le 1$ means AUV will collide with an obstacle, in which case the safety cost is infinite for penalty. Since (1) considers the puffing treatment of obstacles, the path is considered safe as long as it does not intersect with any obstacle, which also guarantees the path's following characteristic. Then the whole fitness function is established as (25). The smaller A is, the better the path is.

$$A = \eta_1 A_1 + \eta_2 A_2 + A_3 \tag{25}$$

4) GENETIC OPERATORS

a: SELECTION

We combine elitist preservation strategy with roulette selection method to conduct the selection. In order to ensure that the optimal individuals must be selected and not destroyed, all individuals are ranked according to their fitness before selection and the top 10% of the individuals are remained. Then the remaining 90% of individuals are selected from the entire population by roulette principle. The selection probability of the ith individual is:

$$P_{\mathrm{si}} = \frac{\frac{1}{A_i}}{\sum_{i=1}^{n} \frac{1}{A_i}} \tag{26}$$

b: CROSSOVER

The top 4% individuals with the best fitness do not participate in the crossover. On one hand, it ensures that the best individuals will not be destroyed, on the other hand, some excellent genes can participate in the crossover operation so that excellent genes can be transmitted in the population. We employ the single-point crossover method. The selected chromosomes are randomly paired and whether executing crossover is determined according to the crossover probability. If the chromosome satisfies the crossover condition, one crossover point is selected randomly and the genes following the selected node will be exchanged.

c: MUTATION

The top 4% individuals also do not participate in the mutation. Alternative-mutation method is used and can be described as that a gene of an individual who meets the mutation condition is randomly selected and changed according to the preset mutation probability. The value after mutation needs to meet the requirement of (19).

5) TERMINATION CONDITION

We employ a dynamic iteration number. When the fitness of the best individual in the current population is constant for three consecutive generations, the cycle is terminated. Therefore, we only need to set the maximum number of iterations. The loop can be automatically terminated after the optimal value is stable, which could avoid wasting time.

B. IMPROVED GA

Better solutions are usually found among new individuals. From the perspective of GA's ability to generate new individuals, crossover is the staple way. Because of the low probability of mutation, the ability of mutation to generate new individuals is quite limited. Moreover, there is a high probability that the mutation will produce an infeasible path, which makes the mutation less effective. In addition, the specificity of the coding way and the single-point crossover method in this paper determine that the genes in the population are determined at the time of initialization. Although the genes of organisms in nature are basically fixed, thanks to the large number of genes in the natural world, various of individuals can be obtained only by crossing. But the initial genes generated by computer is limited, the diversity of population decreases rapidly after a high-probability choice and a low-probability of mutation. These limited genes restrict the possibility of obtaining a better solution. As a result, it is necessary to improve the mutation strategy so that with the help of mutation GA could get favorable genes as much as possible. At the same time, the mutation probability should be increased to continuously enrich the gene pool of the population.

Grey wolf optimization (GWO) [22] is a new type of swarm bionic algorithm, which imitates the predation strategy of the grey wolf in nature and considers the strict hierarchy in the wolves for optimization. When wolves prey on the target, they gradually approached the target under the leadership of three headed wolves. Because it completely depends on the known optimal solution, it has the deficiencies of low solution accuracy, premature and weak local search ability. However, the guidance of the headed wolves in the GWO algorithm hierarchy is worth learning. If it is applied to the GA's mutation process, the mutation will always change towards the optimal solution, which can effectively improve the effectiveness of mutation and enrich the diversity of the population.

The low value of the mutation probability is to prevent GA from approaching the inefficient pure random search algorithm. Besides, the genes generated by mutation are not always useful and may even destroy the excellent individuals. However, after the GWO is used to improve the mutation operator, this problem no longer exists. In addition, although the probability of mutation in nature is low, the actual number of mutation genes is not small thanks to the large number of

its base. Therefore, in order to enrich the number of beneficial genes among the population, the mutation probability in the IGA should be appropriately larger than before. The specific improvement strategy begins with the behavior of the grey wolf approaching the target:

$$C_{\mathrm{i}}^{d}(g+1) = C_{\alpha}^{d}(g) - (2a \cdot rand_1 - a)\left|2 \cdot rand_2 C_{\alpha}^{d}(g) - C_{i}^{d}(g)\right| \tag{27}$$

where $C_\alpha(g)$ is the current optimal individual, $C_i(g)$ is any individual in this case, d is any gene of an individual, variable a linearly decreases from 2 to 0, $rand_1, rand_2 \in [0, 1]$ are random numbers. The improved mutation operation is:

$$C_{i}^{d}(g+1) = \sum_{j=1}^{3} \gamma_j C_{ij}^{d}(g+1) \quad d = 1, 2, 3, 4 \tag{28}$$

$$\gamma_j = \frac{A_{ij}}{A_{\mathrm{i}1} + A_{i2} + A_{i3}}, \quad j = 1, 2, 3 \tag{29}$$

$$\begin{cases} C_{\mathrm{i}1}^{\mathrm{d}}(g+1) = C_{\alpha 1}^{d}(g) - a \cdot (rand_1 - 0.5) \cdot \left|C_{\alpha 1}^{d}(g) - C_{\mathrm{i}}^{d}(g)\right| \\ C_{\mathrm{i}2}^{d}(g+1) = C_{\alpha 2}^{d}(g) - a \cdot (rand_1 - 0.5) \cdot \left|C_{\alpha 2}^{d}(g) - C_{\mathrm{i}}^{d}(g)\right| \\ C_{\mathrm{i}3}^{d}(g+1) = C_{\alpha 3}^{d}(g) - a \cdot (rand_1 - 0.5) \cdot \left|C_{\alpha 3}^{d}(g) - C_{\mathrm{i}}^{d}(g)\right| \end{cases} \tag{30}$$

where $C_{\alpha 1}, C_{\alpha 2}, C_{\alpha 3}$ are the top three optimal individuals respectively, $\gamma_1, \gamma_2, \gamma_3$ are the corresponding weight coefficients. Equation (30) determines that each mutation individual will mutate towards the three optimal individuals, and the impact of the optimal individual is related to the weight coefficients, i.e., the value of fitness. The final IGA flow diagram is shown in Fig.7.

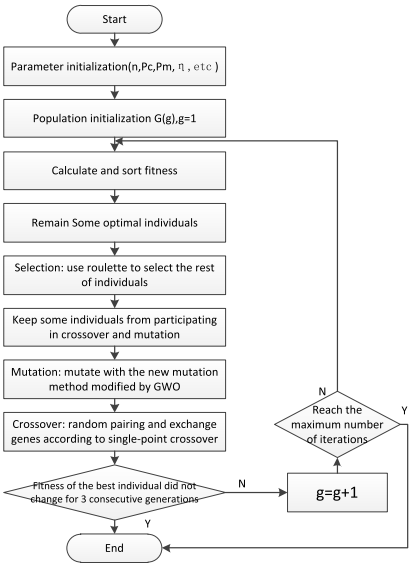

FIGURE 7. Flow diagram of IGA.

V. DYNAMIC IIFDS FOR DYNAMIC THREATS

IIFDS has the advantages of low computational complexity and high computational efficiency, so it can be applied to real-time path planning. Reference [23] constructed a relative flow field based on the relative velocity method and used the IIFDS to avoid dynamic threats as well as obtained a feasible path. However, this method requires higher AUV speed performance, and the continuous adjustment of speed will cause extra energy consumption. This paper combines IIFDS with a reverse-avoidance strategy for real-time path planning to avoid dynamic threats. This method allows AUV to navigate at a constant speed and to avoid dynamic threats relying solely on planning a security path.

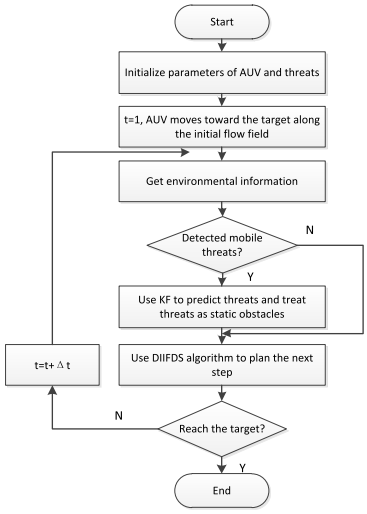

FIGURE 8. Flow diagram of dodging dynamic threats.

Consider the environment where only dynamic threats exist. In a 3-D space, dynamic threats are equivalent to spheres of radius r. When the dynamic threat does not enter the AUV planning area, the AUV moves in a straight line towards the target point. Once the dynamic threat affects the planning area, it begins to process the dynamic threat. The specific process is shown in Fig.8.

Assume that the position, velocity, and other parameters can be obtained through a 3-D underwater target tracking system [24], [25] or by sensors carried by the AUV itself. In order to avoid the obstacles in advance, Kalman filter (KF) is used to predict the motion state of dynamic threats [26]. For the case when the dynamic threat's velocity contains components perpendicular to the AUV velocity, the tangential direction coefficient of IIFDS plays a critical role in the safety of the path. Set $\mathbf{v}$ as a vector of 90° clockwise with the global initial flow field velocity in the x-y plane, as shown by the dotted vector in Fig.9. We can get $\mathbf{v}$ with $d_{xy} = \sqrt{(x_d - x)^2 + (y_d - y)^2}$:

$$\mathbf{v} = \left(\frac{y_d - y}{d_{xy}}, -\frac{x_d - x}{d_{xy}}\right) \tag{31}$$

$\mathbf{u}$ is obstacle's velocity. Assuming that the angle between $\mathbf{u}$ and $\mathbf{v}$ in the x-y plane is β, the tangential direction coefficient θ should be chosen according to (32) so that the AUV will avoid the obstacle in the opposite direction of the

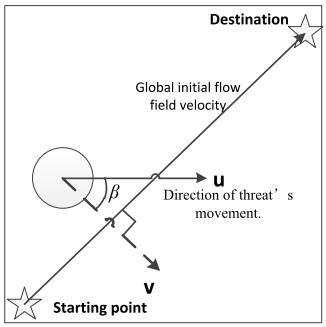

FIGURE 9. Tangential direction coefficient selection condition diagram.

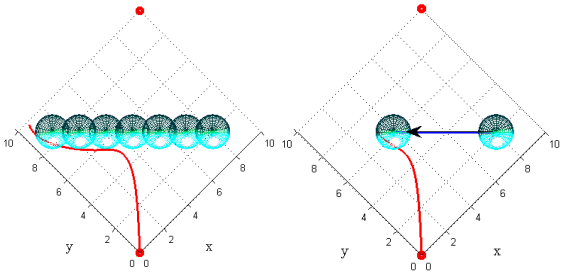

FIGURE 10. Avoiding a dynamic threat in the same direction. (a) "obstacle-following" situation. (b) Collided by the obstacle.

obstacle's movement. The simplified diagram is shown in Fig.9. If the obstacle moves to the lower right, the AUV should move to the upper left to avoid the obstacle, i.e., to avoid the obstacle in the opposite direction. Otherwise, when the speed of the obstacle is similar to the AUV's speed, "obstacle-following" may occur because it is hard for AUV to overtake the obstacle (Fig.10 (a)); when the AUV speed is not fast enough, it may also be threatened by the dynamic threat (Fig.10 (b)). If the AUV moves towards the opposite direction to obstacle in advance, it can easily avoid the above obstacles. Because we plan paths in 3-D space, it also maintains the advantage of being able to avoid obstacles from above or below.

$$\begin{cases} \dfrac{\pi}{2} \le \theta \le \pi, & \text{if } 0 \le |\beta| < \dfrac{\pi}{2} \\ 0 \le \theta < \dfrac{\pi}{2}, & \text{otherwise} \end{cases} \tag{32}$$

VI. SIMULATION

A. STATIC OBSTACLES

A static scenario with dense obstacles is first simulated, and there are overlapping hazardous areas. The horizontal area is 10×11km, and the vertical height is determined by obstacles and paths. Suppose that the starting point is $P_s = (0, 0, 1)$ km, the target point is $P_d = (10, 11, 0.8)$ km, $\Delta t = 6$s, and AUV's speed is constant at 2m/s. Three sets of repulsive reaction coefficient ρ, tangential reaction coefficient σ, tangential direction coefficient θ were randomly selected for IIFDS simulation. The simulation results are shown in Fig.11. It can

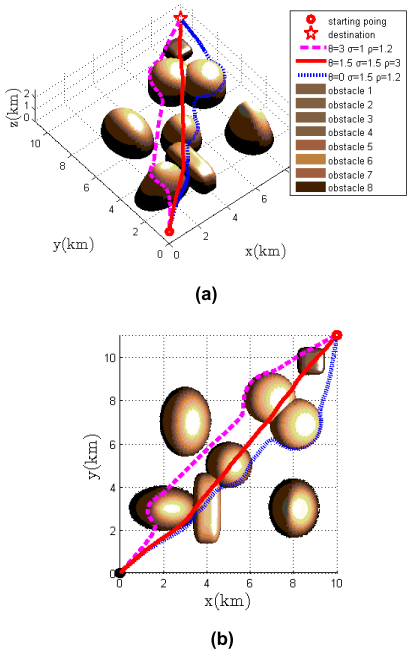

FIGURE 11. Path comparison between IIFDS and A*. (a) 3-D view. (b) Top view.

be seen that the path planned by IIFDS can avoid all obstacles and eventually converge to the destination successfully. The paths have the smooth characteristic of flowing water.

To verify the superiority and effectiveness of the IIFDS, it is compared with A* algorithm in the same environment. Suppose that the size of area is (10,10,1.5) km, the starting position is (0,0,0.5) km, the target position is (10,10,0.5) km and $\rho = 1.1$, $\sigma = 1.1$, $\theta = 0$. The heuristic of the A* uses the Manhattan method and only plans on the horizontal plane. The area is rasterized into 100*100 grids. The planned path is shown in Fig.12. It is apparent that even though both of them successfully reach the destination, the path generated by the A* has sharper turns near obstacles, such as A, B, C in Fig.12 (b). If the AUV has poor maneuverability, the path needs additional smoothing. Whereas the path generated by the IIFDS is smoother, with better security and feasibility. Besides, the paths length of IIFDS and A* are 15 km and 16.8 km respectively, so the quality of path generated by the IIFDS is better overall.

B. PATH OPTIMIZATION

The ocean current adopts the meander shown in Fig.5 and the maximum speed is 2m/s. Assume that there is only horizontal current at different depths, i.e., the z-axis velocity component of the current is 0. From (18), the current velocity $\mathbf{V} = 2 \cdot (-\frac{\partial F}{\partial y}, \frac{\partial F}{\partial x}, 0)$ m/s is obtained. Set V_0 equal to the current maximum velocity so that the initial flow field velocity and current velocity have the same magnitude. To accelerate the simulation speed, set $\Delta t = 30$s. GA parameters are set as follows: the population size $n = 100$, the maximum number of iterations is 30, the crossover probability $P_c = 0.5$, the GA

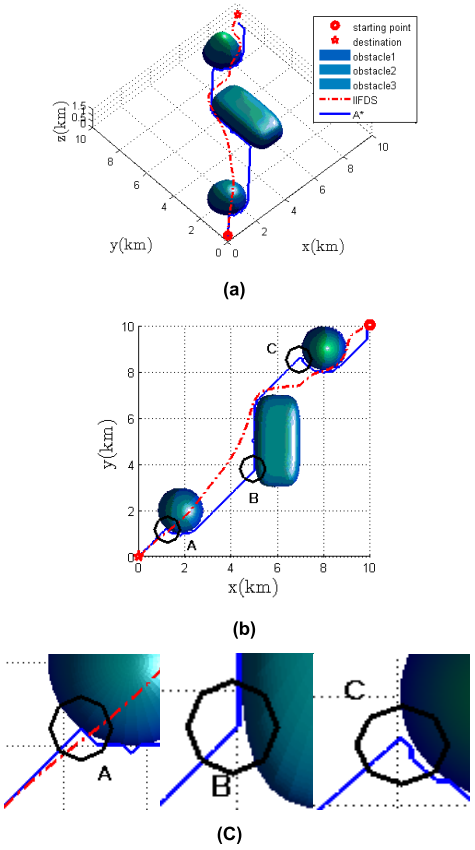

FIGURE 12. Path comparison between IIFDS and A*. (a) 3-D view. (b) Top view. (C) Partial enlargement.

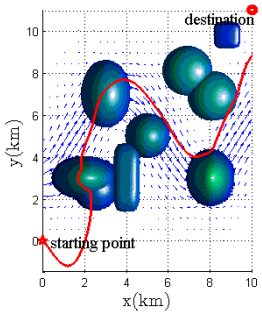

FIGURE 13. AUV cannot reach the point when $\lambda = 0$.

mutation probability $P_{m1} = 0.01$, the IGA mutation probability $P_{m2} = 0.5$. The other parameters remain unchanged. In this simulation, it is considered that when the difference between the fitness of the best individuals in adjacent two generations is less than 0.001, the fitness does not change.

For the value of the fitness coefficient η_1, η_2, different relative values are selected to simulate firstly so that we can intuitively observe the effect. Table 1 shows the comparison between specific simulation results. It can be seen from the table that the smaller η_1/η_2 is, the larger A_1 is, i.e., the longer the path is, the closer to 0 λ is, and the smaller the cost of the angle is. But λ will not be equal to 0, because AUV cannot reach the target point only by means of current (Fig.13).

TABLE 1. Impact of different fitness coefficients.

Fitness coefficients	η_1/η_2	$\eta_1 A_1$	$\eta_2 A_2$	A_2	λ
η_1=1, η_2=0	∞	15.90	0	1.12	0.94
η_1=10, η_2=1	10	158.40	1.07	1.07	0.94
η_1=1, η_2=1	1.00	16.08	1.01	1.01	0.88
η_1=1, η_2=5	0.20	16.44	3.85	0.77	0.52
η_1=1, η_2=10	0.10	16.68	7.6	0.76	0.46
η_1=1, η_2=20	0.05	21.48	10.8	0.54	0.17
η_1=1, η_2=100	0.01	22.9	42	0.42	0.08
η_1=0, η_2=1	0	0	0.45	0.45	0.08

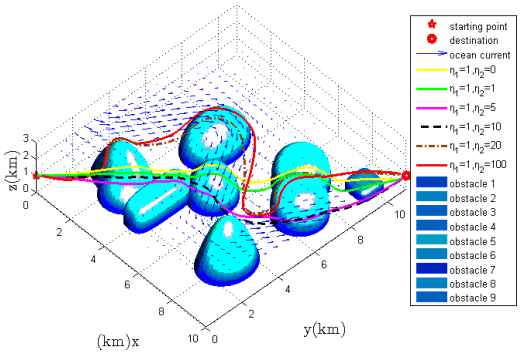

FIGURE 14. Comparison of paths when choosing different fitness coefficients.

The typical path is plotted in Fig.14. It can also be seen clearly that the smaller the ratio of η_1 and η_2 is, the more downstream the path is but the longer the path is.

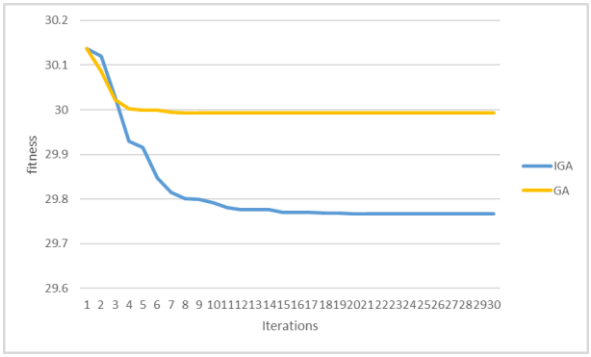

FIGURE 15. Comparison of the best fitness changes in each generation of GA and IGA, averaged over an ensemble of ten simulations.

Set $\eta_1 = 1, \eta_2 = 20$. The individuals with the best fitness in each generation are selected and the fitness of these optimal individuals are plotted as a line chart so that we can clearly see the changes of fitness during the simulation. To get more general results, the average result from 10 runs by GA and IGA are shown in Fig.15. As the number of iterations increases, both fitness tend to evolve toward better overall and eventually converge to feasible optimal solutions. However, GA is prone to converge prematurely, resulting in no further optimization. Whereas IGA significantly improves

TABLE 2. Comparison of GA and IGA.

Algorithm	Optimal convergence value(fitness)	Average optimal value
GA	29.73	29.99
IGA	29.49	29.77

convergence speed and average optimal convergence value. Table 2 gives the specific numerical comparisons, where the optimal convergence value refers to the optimal value that appears in all 10 simulations and the average optimal value refers to the average value of 10 optimal values.

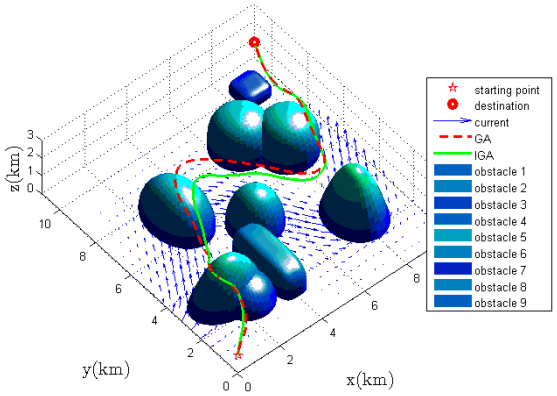

FIGURE 16. Comparison of the optimal paths of IGA and GA.

The best path of IGA is shown in red solid line in Fig.16. In the marine 3-D environment where the current is meandering, although this path is not the shortest one, it is obvious that it can make the AUV sail downstream. Therefore, this is a comprehensive result considering the path's length and energy. The optimal path of GA is also shown in Fig.16 and it can be seen that there are some differences from the comparison. The path of the IGA is closer to the expectation, but both are able to obtain safe, viable and energy-optimal paths with consistency. In a word, the IGA not only retains the optimization features of the original GA, but also obtains better convergence values.

C. AVOIDING DYNAMIC THREATS

Consider the dynamic threats of uniform linear motion. Suppose that the size of the area is $10 \times 10 \times 4$km, the dynamic threat emerges from the point (8, 2, 1)km and will not stop until it reaches the boundary of the area, the radius of its affected area is 1km and it moves with a constant velocity and direction $u = (-0.9, 0.9, 0.01)$m/s; AUV sails at a constant speed of 2m/s, the time interval between adjacent points $\Delta t = 6$s; the starting point $P_s = (0, 0, 1)$km, target point $P_d = (10, 10, 1)$km. Due to the specific nature of IIFDS, it is possible to avoid obstacles in advance by adjusting the repulsive and tangential reaction coefficients, so it is not necessary to predict excessively inaccurate information. Select a prediction width of 5 and the value needs to increase appropriately for larger dynamic threats.

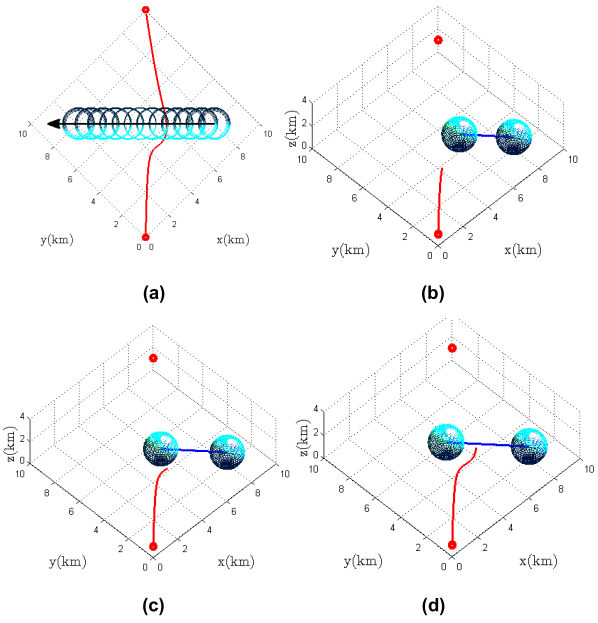

FIGURE 17. The whole path diagram and decomposition diagram avoiding a dynamic threat. (a) The whole path. (b) Time 1. (c) Time 2. (d) Time 3.

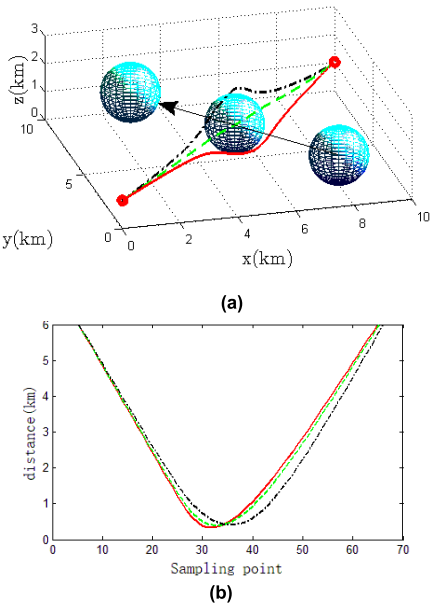

FIGURE 18. The paths planned by IIFDS with reverse-avoidance strategy. (a) Paths. (b) Distances between AUV and the obstacle.

The simulation results are shown in Fig.17, and (a) shows the final result of the simulation. To clearly observe the process, (b-d) show the more detailed movements of the AUV when approaching the obstacle. As can be clearly seen from the figure, the navigation direction is changed in advance as the AUV approaches the obstacle and AUV can bypass the obstacle easily. Then the obstacle will move away automatically. After the obstacle no longer poses a threat, the AUV moves straightly to the target point again. The reverse strategy only stipulates a range of avoidance directions, so the evasion methods are still diverse. Fig.18 shows

several different paths. It can be seen from the distances (b) that all the paths successfully avoid the movement obstacles.

In the presence of current, original convergence and ocean current together determine the new convergence. Suppose that the original convergence's velocity is equal to the current's maximum velocity which is 1.2m/s, current related parameters are $t = 4, c = 1.2, k = 1, e = 0.1$, $b_0 = 1.5, \lambda = 0.6, \varpi = 1.6, \chi = \pi/2$. In order to conduct the comparison fairly, the set of dynamic threat and other parameters are the same as the simulation with no current. The simulation results are shown in Fig.19 and figure (c) means the path is still safe and feasible. Due to the influence of current, the path is longer and more twisted. But the planned path can still safely avoid the dynamic threat, and to some extent, it saves energy by sailing downstream.

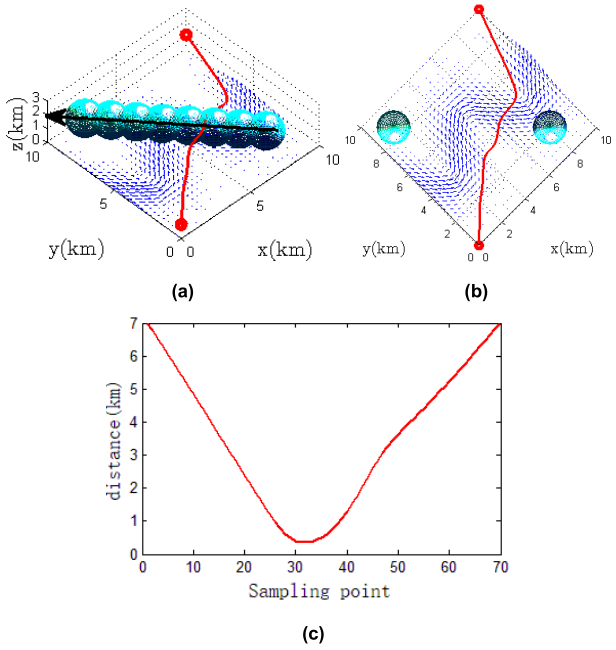

FIGURE 19. Avoiding a dynamic threat in current environment. (a) 3-D view. (b) Top view. (c) Distances between AUV and the obstacle.

When there are multiple dynamic threats in the environment, the simulation results are shown in Fig.20. The distances in Fig.21 demonstrate that the IIFDS method based on the reverse-avoidance strategy can well plan the path when the dynamic threats exist, and the path does not require extra smoothing.

The simulation results when current is added to the environment are shown in Fig.22. Because current is mainly horizontal, it can be seen from the comparison of Fig.22 (a) and (b) that the planned path is greatly influenced by ocean current in the horizontal direction. However, it still successfully avoids all the obstacles (Fig.22 (c)) and there is no sharp turn, which proves the feasibility and certain robustness of the algorithm.

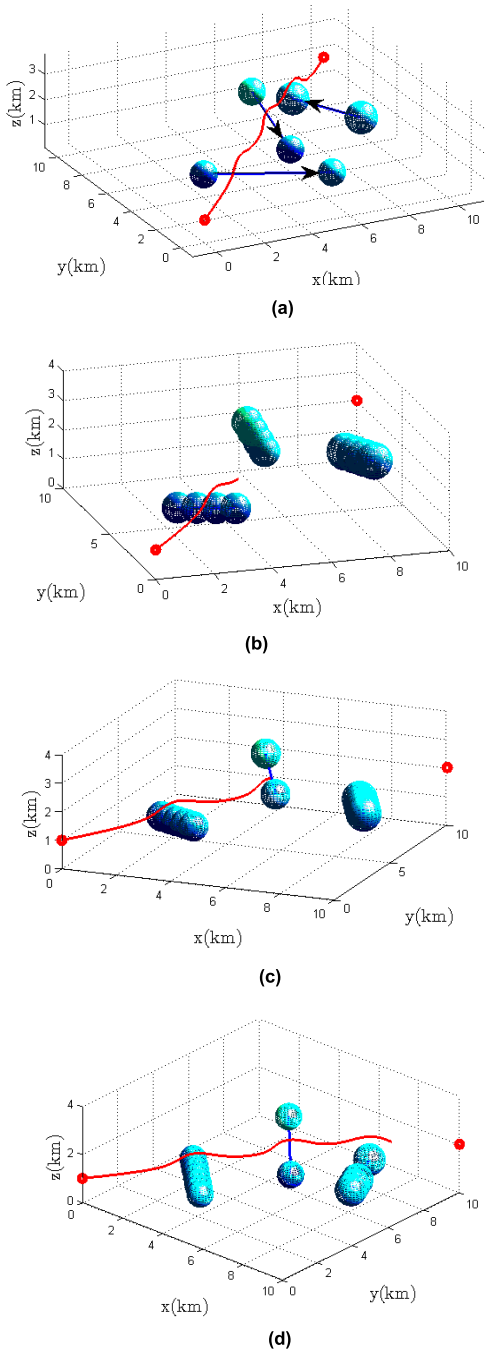

FIGURE 20. Path planned when there are multiple dynamic threats. (a) The whole path. (b) Avoiding the first dynamic threat. (c) Avoiding the second dynamic threat. (d) Avoiding the third dynamic threat.

Avoiding dynamic threats requires high real-time performance. In order to verify the real-time performance of the algorithm, we conduct five different simulations by adjusting the coefficients of IIFDS and record the average time of one step of calculation in each simulation. The platform is configured with 4GB DDR4 memory and the processor is Intel Core I7-6500U. The results are shown in Table 3. It can be seen that thanks to the high computational power of the IIFDS, even if there are three dynamic threats, the single-step

TABLE 3. Average time of each operation in five different simulations.

	Simulation	1	2	3	4	5	Average
Time (s)	1 obstacle	0.00169	0.00180	0.00200	0.00179	0.00185	0.00183
	3 obstacles	0.00277	0.00287	0.00270	0.00283	0.00272	0.00278

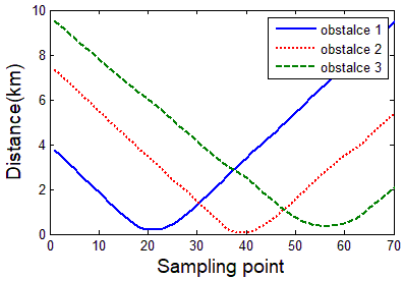

FIGURE 21. Distances between AUV and three dynamic threats. (No current).

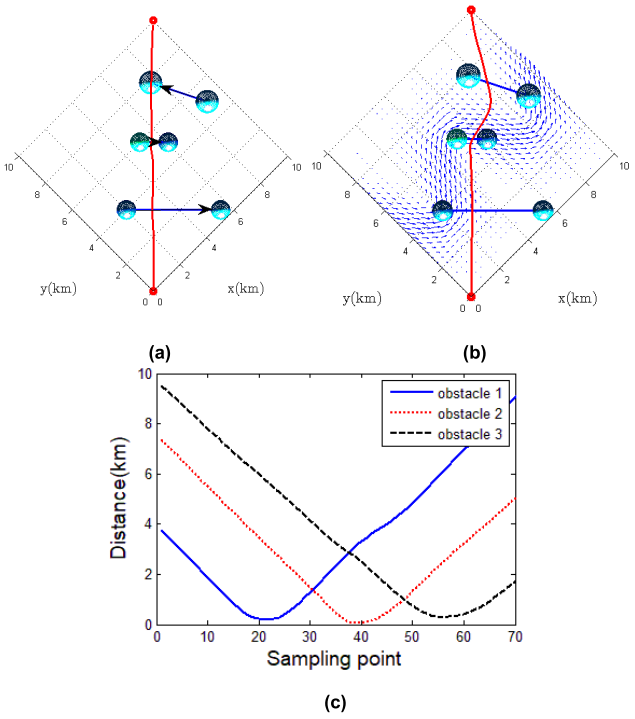

FIGURE 22. Path planned when there are multiple dynamic threats and current. (a) No current. (b) With current. (c) Distances between AUV and three dynamic threats. (With current).

operation time is much shorter than the unit interval of 6 s. Therefore, it can completely meet the real-time requirements of avoiding dynamic threats.

Finally, the IIFDS method is verified in a complex environment with current, static and dynamic threats simultaneously. Given the starting point $P_s = (0, 0, 1)$ km and the destination $P_d = (10, 10, 1.5)$ km, the other parameters are unchanged. A feasible path is also obtained, as shown in Fig.23.

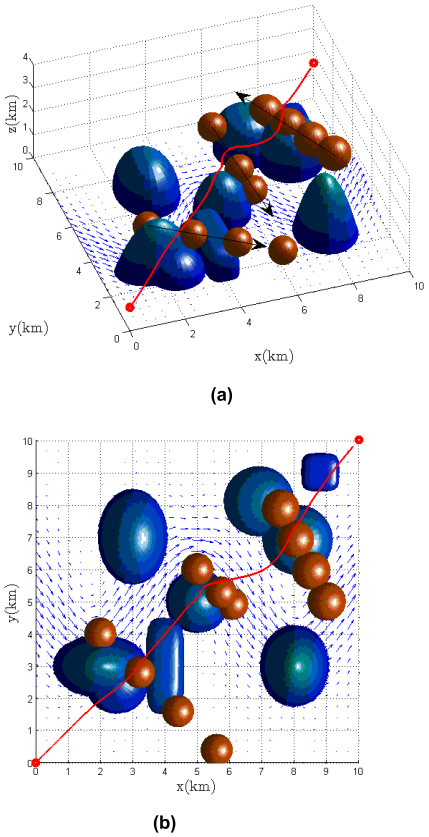

FIGURE 23. Path planned in a complex environment with current, static and dynamic threats simultaneously. (a) 3-D view. (b) Top view.

VII. CONCLUSION

This paper applies the IIFDS to AUV 3-D path planning in the environment with complex static obstacles, ocean current and dynamic threats. The path planned by IIFDS is smooth and flexible. With the introduction of the flow field weight coefficient, the algorithm can reasonably balance the length of path with the utilization of current. The energy-optimal path obtained by IGA can make the AUV navigate as downstream as possible while keeping the path as short as possible. When there are simple dynamic threats in the environment, a feasible path can be obtained using IIFDS combined with reverse-avoidance strategy. As obstacles are virtual, the current is not affected by obstacles in this paper. It does not accord with the actual situation, so we will consider the impact of obstacles on current in future studies.

REFERENCES

[1] M. Liu, B. Xu, and X. Peng, "Cooperative path planning for multi-AUV in time-varying ocean flows," *J. Syst. Eng. Electron.*, vol. 27, no. 3, pp. 612–618, 2016.

[2] J. J. Kuffner and S. M. Lavalle, "RRT-connect: An efficient approach to single-query path planning," in *Proc. IEEE Int. Conf. Robot. Autom. (ICRA)*, Apr. 2002, pp. 995–1001.
[3] V. Roberge, M. Tarbouchi, and G. Labonte, "Comparison of parallel genetic algorithm and particle swarm optimization for real-time UAV path planning," *IEEE Trans. Ind. Informat.*, vol. 9, no. 1, pp. 132–141, Feb. 2013.
[4] G. C. S. Cruz and P. M. M. Encarnação, "Obstacle avoidance for unmanned aerial vehicles," *J. Intell. Robot. Syst.*, vol. 65, nos. 1–4, pp. 203–217, 2012.
[5] A. Pereira *et al.*, "Toward risk aware mission planning for autonomous underwater vehicles," in *Proc. IEEE/RSJ Int. Conf. Intell. Robots Syst.*, Sep. 2011, pp. 3147–3153.
[6] C. Petres, Y. Pailhas, P. Patron, Y. Petillot, J. Evans, and D. Lane, "Path planning for autonomous underwater vehicles," *IEEE Trans. Robot.*, vol. 23, no. 2, pp. 331–341, Apr. 2007.
[7] A. A. Pereira, J. Binney, G. A. Hollinger, and G. S. Sukhatme, "Risk-aware path planning for autonomous underwater vehicles using predictive ocean models," *J. Field Robot.*, vol. 30, no. 5, pp. 741–762, 2013.
[8] T. Lolla, M. P. Ueckermann, K. Yiğit, P. J. Haley, and P. F. J. Lermusiaux, "Path planning in time dependent flow fields using level set methods," in *Proc. IEEE Int. Conf. Robot. Autom.*, May 2012, pp. 166–173.
[9] T. Lolla, P. F. J. Lermusiaux, M. P. Ueckermann, and P. J. Haley, "Time-optimal path planning in dynamic flows using level set equations: Theory and schemes," *Ocean Dyn.*, vol. 64, no. 10, pp. 1373–1397, 2014.
[10] Z. Zeng, A. Lammas, K. Sammut, and F. He, "Optimal path planning based on annular space decomposition for AUVs operating in a variable environment," in *Proc. IEEE Auton. Underwater Vehicles*, Sep. 2012, pp. 1–9.
[11] Z. Zeng, A. Lammas, K. Sammut, F. He, and Y. Tang, "Shell space decomposition based path planning for AUVs operating in a variable environment," *Ocean Eng.*, vol. 91, pp. 181–195, 2014.
[12] S. M. Khansari-Zadeh and A. Billard, "A dynamical system approach to realtime obstacle avoidance," *Auton. Robots*, vol. 32, no. 4, pp. 433–454, 2012.
[13] S. M. Khansarizadeh and A. Billard, "Realtime avoidance of fast moving objects: A dynamical system-based approach," in *Proc. Electron. Workshop Robot Motion Planning, Online, Reactive, Real-Time*, 2012.
[14] X. Zhong and X. Peng, "Velocity-change-space-based dynamic motion planning for mobile robots navigation," *Neurocomputing*, vol. 143, no. 2, pp. 153–163, 2014.
[15] S. Akishita, T. Hisanobu, and S. Kawamura, "Fast path planning available for moving obstacle avoidance by use of Laplace potential," in *Proc. IEEE/RSJ Int. Conf. Intell. Robots Syst. (IROS)*, vol. 1, Jul. 1993, pp. 673–678.
[16] S. M. Zadeh, A. M. Yazdani, K. Sammut, and D. M. W. Powers, "Online path planning for AUV rendezvous in dynamic cluttered undersea environment using evolutionary algorithms," *Appl. Soft Comput.*, 2017, doi: 10.1016/j.asoc.2017.10.025.
[17] Z. Zeng, K. Sammut, A. Lammasm, F. He, and Y. Tang, "Efficient path replanning for AUVs operating in spatiotemporal currents," *J. Intell. Robot. Syst.*, vol. 79, no. 1, pp. 135–153, 2015.
[18] H. Wang, L. Wentao, Y. Peng, L. Xiao, and L. Chang, "Three-dimensional path planning for unmanned aerial vehicle based on interfered fluid dynamical system," *Chin. J. Aeronaut.*, vol. 28, no. 1, pp. 229–239, 2015.
[19] P. Yao, H. Wang, and Z. Su, "UAV feasible path planning based on disturbed fluid and trajectory propagation," *Chin. J. Aeronaut.*, vol. 28, no. 4, pp. 1163–1177, 2015.
[20] A. Alvarez, A. Caiti, and R. Onken, "Evolutionary path planning for autonomous underwater vehicles in a variable ocean," *IEEE J. Ocean. Eng.*, vol. 29, no. 2, pp. 418–429, Apr. 2004.
[21] B. Garau, M. Bonet, A. Alvarez, and S. Ruiz, "Path planning for autonomous underwater vehicles in realistic oceanic current fields: Application to gliders in the Western Mediterranean Sea," *J. Maritime Res.*, vol. 6, no. 2, pp. 5–22, 2009.
[22] S. Mirjalili, S. M. Mirjalili, and A. Lewis, "Grey wolf optimizer," *Adv. Eng. Softw.*, vol. 69, pp. 46–61, Mar. 2014.
[23] P. Yao, H. Wang, and C. Liu, "3-D dynamic path planning for UAV based on interfered fluid flow," in *Proc. IEEE Chin. Guid., Navigat. Control Conf.*, Aug. 2014, pp. 997–1002.
[24] Z. Wu and X. Li, "An improved underwater acoustic network localization algorithm," *China Commun.*, vol. 12, no. 3, pp. 77–83, Mar. 2015.
[25] X. Tan and J. Li, "Cooperative positioning in underwater sensor networks," *IEEE Trans. Signal Process.*, vol. 58, no. 11, pp. 5860–5871, Nov. 2010.
[26] M. Kang, Y. Liu, and Y. Zhao, "A threat modeling method based on Kalman filter for UAV path planning," in *Proc. IEEE Control Decis. Conf.*, May 2017, pp. 3823–3828.

PENG YAO was born in Shandong, China, in 1989. He received the B.S. degree from the School of Control Science and Engineering, Shandong University, Jinan, China, and the Ph.D. degree from the School of Automation Science and Electrical Engineering, Beihang University, Beijing, China, in 2011 and 2017, respectively.

In 2017, he joined the College of Engineering, Ocean University of China, where he is currently a Lecturer. His current research interests include path planning and intelligent decision of unmanned vehicle, cooperative optimization, and control of multi-agents.

SHIQIANG ZHAO was born in Shandong, China, in 1996. He received the B.S. degree from the College of Engineering, Ocean University of China, Qingdao, China, in 2018.